Available online at www.sciencedirect.com
ScienceDirect
Wave Motion 43 (2006) 631–645
WAVE MOTION
www.elsevier.com/locate/wavemoti

Diffraction by a convex polygon with side-wise constant impedance

Bair V. Budaev *, David B. Bogy

Department of Mechanical Engineering, University of California, Berkeley, CA 94720, USA

Received 13 January 2006; received in revised form 9 May 2006; accepted 25 May 2006
Available online 1 August 2006

Abstract

The recently developed probabilistic approach to wave propagation and diffraction is applied to the two-dimensional problem of diffraction by an arbitrary convex polygon with side-wise constant impedance boundary conditions. Surprisingly, the new method provides a rigorous solution which is simple, transparent and complimentary to the ray approximation. It is easy to implement and it is compatible with intuitive ideas about diffraction. The numerical examples confirm the feasibility of the solution.

Keywords: Wave propagation; Diffraction; Ray method; Brownian motion; Stochastic processes

1. Introduction

The theory of wave propagation has traditionally considered problems of diffraction by simplified objects which permit exact closed-form solutions. The first problem of this kind was solved in the 1890s, when Poincaré [11,12] and Sommerfeld [13] independently explicitly described the waves generated by a plane incident wave in an infinite wedge with ideally reflecting faces. After that, many other problems of diffraction were solved analytically, and the interest in such solutions was boosted by the development of the geometrical theory of diffraction [9], which heavily uses the diffraction coefficients derived from the analysis of wave fields in canonical domains.

The pioneering papers of Poincaré and Sommerfeld not only presented explicit solutions of the diffraction problem, but they also presented two different approaches. Thus, Poincaré employed the method of separation of variables and Sommerfeld represented the solution by the so-called Sommerfeld integral, which was equivalent to using the integral Mellin transform. For more than a century the methods of separation of variables and integral transforms have remained the primary approaches to closed-form solutions in the theory of diffraction, which remarkably confirms the power of these methods, but which also explains why closed-form solutions are

* Corresponding author. Tel.: +1 510 643 5776; fax: +1 510 642 6163.
E-mail addresses: budaev@berkeley.edu (B.V. Budaev), dbogy@cml.me.berkeley.edu (D.B. Bogy).

0165-2125/$ - see front matter © 2006 Elsevier B.V. All rights reserved.
doi:10.1016/j.wavemoti.2006.05.007

mostly available for problems with a limited (small) number of scatterers. Indeed, these methods are best suited to problems in domains which are bounded by the coordinate surfaces of common coordinate systems, such as Cartesian, polar, spherical, elliptic, or some other classical coordinates, which permit explicit representations for the eigenfunctions of the Laplace operator. For example, the problems of diffraction by an infinite wedge or by a cylinder can be explicitly solved in polar coordinates, and the problems of diffraction by a circular cone or by a sphere can be solved using spherical coordinates. On the other hand, there are no suitable coordinates for a truncated wedge, and the problem of diffraction by a truncated wedge does not have a conventional closed-form solution. Nevertheless, the availability of explicit representations for wave fields in canonical domains made it possible to address problems of diffraction by scatterers of rather general shape. Thus, in [10] the problem of diffraction of an incident impulse by an ideally reflecting convex polygon solved by sequential iterations, as a wave hit one vertex after another. More recently [1,7], problems of diffraction by polygonal objects were addressed by techniques developed for the analysis of wave propagation in infinite wedges.

The above mentioned analytic approaches to problems of diffraction were recently complimented by a new method, based on rather well-known probabilistic random walk approaches to elliptic and parabolic partial differential equations [6,8]. These methods have already been successfully applied to the problem of diffraction by a plane angular sector [2] and to the problem of diffraction by an infinite wedge with anisotropic face impedances [3]. Although these are problems with canonical geometries, which may be addressed by conventional techniques, the obtained probabilistic solutions look attractive because of their transparency and simplicity. Most recently, the random walk method was applied to two-dimensional problems of diffraction by a half space with piece-wise constant impedances, and by a line segment with faces that have different constant impedances. These problems do not have known conventional closed-form solutions, but the probabilistic solutions obtained in [5] are not considerably more complex that the solutions of the other problems mentioned above.

Here, we apply the random walk method to the two-dimensional problem of diffraction by an arbitrary convex polygon with side-wise constant boundary impedances. We follow closely the method from [5] and obtain a theoretically exact solution of a wide class of problems. The paper contains two main sections. The first section is devoted to the formalization of the problem and to the development of the appropriate notation. Then, in the second section, the formulated problem is solved by the random walk method. The feasibility of the obtained solution is illustrated by its application to two different pentagons for which numerical results are presented in the third section.

2. Formulation of the problem

2.1. Geometry

To solve or even formulate the problem of diffraction by a polygon we need to develop some convenient notation which simplifies the description of wave fields in the exterior of a convex polygon.

Let G be the exterior of the convex polygon Γ with consequential vertices $O_1, O_2, \ldots, O_N$ enumerated in the counter-clockwise direction, as shown in Fig. 1. For convenience we adopt the periodicity convention

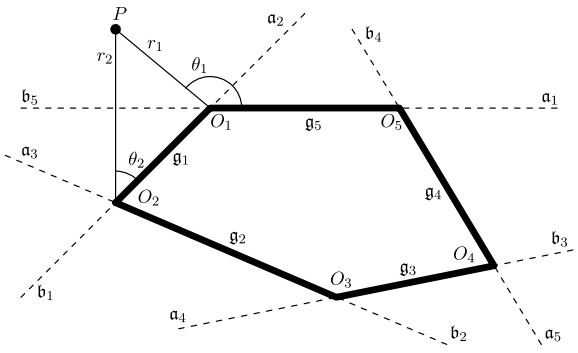

Fig. 1. Geometry of a polygon.

$$O_{n+N} \equiv O_n, \tag{2.1}$$

which makes the symbol O_n meaningful for any integer n. The exterior wedge at the vertex O_n is denoted as $\mathfrak{O}_n$, and the sides $\mathfrak{g}_n$ of the polygon are defined as the segments $\mathfrak{g}_n = (O_n, O_{n+1})$. The length of the side $\mathfrak{g}_n$ and the angle of the wedge $\mathfrak{O}_n$ are denoted as L_n and α_n, so that

$$L_n = \|O_{n+1} - O_n\|, \qquad \alpha_n = \mathrm{meas}(\mathfrak{O}_n). \tag{2.2}$$

We will simultaneously use several coordinate systems in the exterior domain G. The standard polar coordinates (r,θ) will be used as a universal reference system, but we will also use the polar coordinates (r_n,θ_n) centered at the vertices O_n and calibrated by the conditions $\theta_n(O_{n-1}) = 0$. This implies that the segments $\mathfrak{g}_{n-1}$ and $\mathfrak{g}_n$ are described as

$$\begin{aligned} &\mathfrak{g}_{n-1}: \quad \theta_n = 0, \quad \theta_{n-1} = \alpha_{n-1}, \\ &\mathfrak{g}_n: \quad \theta_n = \alpha_n, \quad \theta_{n+1} = 0, \end{aligned} \tag{2.3}$$

and that the conditions

$$\begin{aligned} &\mathfrak{a}_n: \quad \theta_n = 0, \quad \theta_{n-1} = \alpha_{n-1} - \pi, \\ &\mathfrak{b}_n: \quad \theta_n = \alpha_n, \quad \theta_{n+1} = \pi, \end{aligned} \tag{2.4}$$

determine the rays which compliment $\mathfrak{g}_{n-1}$ and $\mathfrak{g}_n$ to the faces $\theta_n = 0$ and $\theta_n = \alpha_n$ of the wedge $\mathfrak{O}_n$, respectively. The rays $\mathfrak{a}_n$ and $\mathfrak{b}_n$ are shown in Fig. 1 by dashed lines.

Since different coordinates (r_n,θ_n) refer to the same point of the plane, there is a one-to-one correspondence between any pair of such coordinates. For example, applying the cosine theorem to the triangles $O_{n-1}PO_n$ and $O_n\,PO_{n+1}$, where P is the observation point, it is easy to show that the coordinates r_{n+1} and r_{n-1} are related to (r_n,θ_n) through the analytic expressions

$$\begin{aligned} &r_{n-1} = \mathscr{R}(r_n, \theta_n, -L_{n-1}), && \theta_{n-1} = \mathscr{F}(r_n, \theta_n, -L_{n-1}), \\ &r_{n+1} = \mathscr{R}(r_n, \theta_n - \alpha_n + \pi, L_n), && \theta_{n+1} = \mathscr{F}(r_n, \theta_n - \alpha_n + \pi, L_n), \end{aligned} \tag{2.5}$$

where

$$\mathscr{R}(r,\theta,L) = \sqrt{r^2 + 2rL\cos\theta + L^2}, \qquad \mathscr{F}(r,\theta,L) = \arccos\left(\frac{r\cos\theta + L}{\mathscr{R}(r,\theta,L)}\right). \tag{2.6}$$

The polar coordinates (r_n,θ_n) provide a convenient analytic description of the sides $\mathfrak{g}_n$ and $\mathfrak{g}_{n-1}$ of the polygon. Indeed, combining (2.3) with (2.5) we obtain the formulas

$$\begin{aligned} &\mathfrak{g}_{n-1}: \quad \theta_n = 0, \quad \mathscr{F}(r_n, \theta_n, -L_{n-1}) = \alpha_{n-1}, \\ &\mathfrak{g}_n: \quad \theta_n = \alpha_n, \quad \mathscr{F}(r_n, \theta_n - \alpha_n + \pi, L_n) = 0, \end{aligned} \tag{2.7}$$

which analytically define segments $\mathfrak{g}_n$ and $\mathfrak{g}_{n-1}$ in the coordinates (r_n,θ_n) centered at the common vertex of these segments. Similarly, the rays $\mathfrak{a}_n$ and $\mathfrak{b}_n$ defined by (2.4) as one-way extensions of the segments $\mathfrak{g}_{n-1}$ and $\mathfrak{g}_n$, can be characterized as

$$\begin{aligned} &\mathfrak{a}_n: \quad \theta_n = 0, \quad \mathscr{F}(r_n, \theta_n, -L_{n-1}) = \alpha_{n-1} - \pi, \\ &\mathfrak{b}_n: \quad \theta_n = 0, \quad \mathscr{F}(r_n, \theta_n - \alpha_n + \pi, L_n) = \pi. \end{aligned} \tag{2.8}$$

Since the functions $\mathscr{R}(r,\theta,L)$ and $\mathscr{F}(r,\theta,L)$ are analytic, the formulas (2.7) and (2.8) define multi-sheet manifolds which analytically continue the segments $\mathfrak{g}_{n-1}$, $\mathfrak{g}_n$ and the rays $\mathfrak{a}_n$, $\mathfrak{b}_n$ to the complex space.

To eliminate or, at least, reduce the ambiguity caused by the simultaneous use of several coordinate systems we include a reference to the coordinate system in the notation for the functions on the plane. Thus, a function in the domain G is denoted hereafter either as $F(\xi,\eta;n)$ or as $F(\xi,\eta)$. In the first case, the index n indicates that the pair (ξ,η) represents the polar coordinates of a certain point in the nth coordinate system (r_n,θ_n), and in the second case, the pair (ξ,η) is considered to be coordinates in the standard system. In particular, this means that $F(\xi,\eta)$, $F(\xi,\eta;n)$ and $F(\xi,\eta;m)$ with $m \neq n$ may not be equal to each other because they represent the same field at different points in the physical space. On the other hand, if (ξ,η), (ξ_n,η_n) and (ξ_m,η_m) are the coordinates of the

same physical point in the standard, in the nth and in the mth coordinate systems, then $F(\xi,\eta)$, $F(\xi_n,\eta_n;n)$ and $F(\xi_m,\eta_m;m)$ are identical to each other because they represent the same field at that physical point.

Finally, it is worth mentioning that due to the periodicity convention (2.1) all of the n-indexed objects introduced above remain meaningful for arbitrary integer values of n.

2.2. Formulation of the problem of diffraction

We assume that each of the sides $\mathfrak{g}_m$ of the polygon Γ has a constant impedance B_m restricted by the condition

$$\mathrm{Re}(B_m) \geqslant 0. \tag{2.9}$$

Then the problem of diffraction of a plane incident wave

$$U_*(r,\theta;t) = \mathrm{e}^{-\mathrm{i}kr\cos(\theta-\theta_*)-\mathrm{i}kt} \tag{2.10}$$

by the polygon Γ consists of the computation of the field $U(r,\theta)$ which is uniquely defined and bounded everywhere in G and satisfies the Helmholtz equation

$$\nabla^2 U + k^2 U = 0 \tag{2.11}$$

complimented by the standard radiation condition and by the impedance boundary conditions

$$\left.\frac{\partial U}{\partial \vec{n}_m} + \mathrm{i}kB_m U\right|_{\mathfrak{g}_m} = 0, \qquad m = 1,2,\ldots,N, \tag{2.12}$$

where $\vec{n}_m$ is a unit normal to $\mathfrak{g}_m$ oriented to the exterior of the polygon.

An elementary geometric-optical analysis supplies a piece-wise continuous wave field U_g which satisfies all of the conditions of the problem, except that it has specific jumps as described below.

Jumps of the geometric field U_g may only occur along several rays originating from the vertices of the polygon, and only a finite number N_μ of the such rays may originate from a particular vertex O_μ. To keep track of these rays, we use a double-indexed notation $\mathfrak{l}^\nu_\mu$, where the lower index corresponds to the vertex O_μ where the ray originates, and the upper index enumerates the rays originating from O_μ. If the polygon is strictly convex, then N_μ may have only two possible values, $N_\mu = 2$ or $N_\mu = 0$. For example, in the configuration shown in Fig. 2, there are no rays $\mathfrak{l}^\nu_\mu$ originating from O_2 and O_3, which means that $N_2 = N_3 = 0$. The rays $\mathfrak{l}^\nu_\mu$ are described in the polar coordinates (r_μ,θ_μ) as

$$\mathfrak{l}^\nu_\mu: \quad r_\mu > 0, \quad \theta_\mu = \phi^\nu_\mu, \tag{2.13}$$

where the angles ϕ^ν_μ are completely determined by the geometry of the problem and are not affected by the impedances B_m. However, the impedances determine the jumps of the geometric field along these rays which are described in the coordinates (r_μ,θ_μ) by the expressions

$$U_g(r_\mu,\phi^\nu_\mu+0;\mu) - U_g(r_\mu,\phi^\nu_\mu-0;\mu) = -K^\nu_\mu Q_\mu \mathrm{e}^{\mathrm{i}kr_\mu}, \tag{2.14}$$

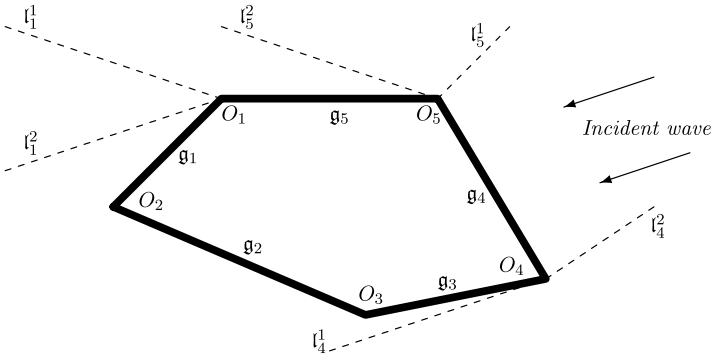

Fig. 2. Discontinuities of the geometric field.

$$\frac{\partial U_g(r_\mu, \phi_\mu^v + 0; \mu)}{\partial \theta_\mu} = \frac{\partial U_g(r_\mu, \phi_\mu^v - 0; \mu)}{\partial \theta_\mu}, \tag{2.15}$$

and

$$Q_\mu = \exp(-\mathrm{i}kr_\mu^o \cos(\theta_\mu^o - \theta_*)), \qquad r_\mu^o \equiv r(O_\mu), \quad \theta_\mu^o \equiv \theta(O_\mu), \tag{2.16}$$

where ϕ_μ^v are the angles from (2.13) and K_μ^v are the coefficients determined by the geometry of the problem and by the boundary impedances. For example, in the configuration shown in Fig. 2 these coefficients are determined as

$$K_1^2 = 1, \quad K_4^2 = -1, \tag{2.17}$$

and

$$K_1^1 = -K_5^2 = \frac{\sin\theta_* - B_5}{\sin\theta_* + B_5}, \qquad K_5^1 = -K_4^1 = \frac{-\sin(\theta_* + \alpha_5) - B_4}{-\sin(\theta_* + \alpha_5) + B_4}. \tag{2.18}$$

As mentioned above, the geometric field U_g obeys all of the conditions of the problem of diffraction by the polygon Γ, except instead of being continuous everywhere in G, it has jumps (2.14) on a finite number $\widetilde{N} = \sum N_\mu$ of rays l_μ^v. Therefore, taking into account the jump conditions (2.14) and (2.15) we may represent the exact solution as a superposition.

$$U(r, \theta) = U_g(r, \theta) + \sum_{\mu=1}^{N} \sum_{v=1}^{N_\mu} U_\mu^v(r, \theta, \phi_\mu^v), \tag{2.19}$$

of the geometric field U_g with $\widetilde{N}$ diffracted fields U_μ^v each of which compensates the jump of the geometric field along one and only one ray l_μ^v. Next assuming that every individual diffracted field is 2π-periodic with respect to the angular coordinate, we arrive at the decomposition

$$U_\mu^v(r, \theta, \phi) = K_\mu^v Q_\mu \sum_{j=-\infty}^{\infty} U_{\mu,\phi}(r, \theta + 2\pi j), \tag{2.20}$$

where $U_{\mu,\phi}(r,\theta)$ is the solution of the following problem.

Problem-I. Find the solution $U_{\mu,\phi}(r,\theta)$ of the Helmholtz equation

$$\nabla^2 U_{\mu,\phi}(r, \theta) + k^2 U_{\mu,\phi}(r, \theta) = 0, \tag{2.21}$$

complimented by the impedance boundary conditions

$$\left.\frac{\partial U_{\mu,\phi}}{\partial \vec{n}} + \mathrm{i}kB_m U_{\mu,\phi}\right|_{\mathrm{g}_m} = 0, \tag{2.22}$$

where m takes any integer value, and by the radiation and interface conditions

$$U_{\mu,\phi}(r_\mu, \theta_\mu; \mu)\mathrm{e}^{-\mathrm{i}kr_\mu} = o(1), \qquad r_\mu \to \infty, \quad \theta_\mu \neq \phi; \tag{2.23}$$

and

$$\begin{aligned} &U_{\mu,\phi}(r_\mu, \phi + 0; \mu) - U_{\mu,\phi}(r_\mu, \phi - 0; \mu) = 1, \\ &\frac{\partial U_{\mu,\phi}(r_\mu, \phi + 0; \mu)}{\partial \theta_\mu} = \frac{\partial U_{\mu,\phi}(r_\mu, \phi - 0; \mu)}{\partial \theta_\mu}, \end{aligned} \tag{2.24}$$

formulated in the coordinates (r_μ,θ_μ).

3. Computation of the diffracted fields

It is clear that formulas (2.19) and (2.20) effectively reduce the original problem of diffraction to the fundamental *Problem-I*, which has to be solved with several sets of parameters μ and ϕ. Therefore, to simplify

the presentation it suffices to limit the rest of the paper to the discussion of the *Problem-I*, where μ and ϕ are considered as given parameters.

3.1. Multiple overlapping representations of the diffracted field

To take full advantage of using several coordinate systems, we seek the solution $U_{\mu,\phi}(r,\theta)$ of the *Problem-I* simultaneously in all of the product forms

$$U_{\mu,\phi}(r,\theta) = u_{\mu,\phi}(r_n,\theta_n;n)\mathrm{e}^{\mathrm{i}kr_n}, \tag{3.1}$$

where (r,θ) are the standard polar coordinates of the observation point and (r_n,θ_n) are the coordinates of the same point in the nth system centered at the vertex O_n. For simplicity, we adopt the abbreviation

$$u(r_n,\theta_n;n) \equiv u_{\mu,\phi}(r_n,\theta_n;n), \tag{3.2}$$

which will be used wherever it does not cause confusion.

It is important to recall that the index n in $u(\xi,\eta;n)$ indicates that the pair (ξ,η) represents the polar coordinates of a certain point in the nth coordinate system (r_n,θ_n). It is also worth mentioning that, although each of the products (3.1) may be used anywhere, the representation in the nth coordinates (r_n,θ_n) will actually be used only inside the wedge $\mathfrak{D}_n$. However, since the wedges with different indices overlap, it is correct to state that we use multiple overlapping representations of the wave fields.

Since all of the products (3.1) represent the same field, the amplitudes $u(r_n,\theta_n;n)$ with different indices n are not independent, but are explicitly related to each other. In particular, the relationships between the amplitude $u(r_n,\theta_n;n)$ and the adjacent amplitudes $u(r_{n\pm1},\theta_{n\pm1};n\pm1)$ are given by the formulas

$$\begin{aligned} u(r_n,\theta_n;n) &= u(r_{n-1},\theta_{n-1};n-1)\mathrm{e}^{\mathrm{i}k(r_{n-1}-r_n)},\\ u(r_n,\theta_n;n) &= u(r_{n+1},\theta_{n+1};n+1)\mathrm{e}^{\mathrm{i}k(r_{n+1}-r_n)}, \end{aligned} \tag{3.3}$$

where $r_{n\pm1}$ and $\theta_{n\pm1}$ are related to (r_n,θ_n) through formulas (2.5). In general, formulas (3.3) are rather complex, but on the rays $\mathfrak{a}_n$ and $\mathfrak{b}_n$ from (2.4) they degenerate to simple expressions

$$\begin{aligned} u(r_n,\theta_n;n) &= u(r_n-L_{n-1},\theta_n+\alpha_{n-1}-\pi;n-1)\mathrm{e}^{-\mathrm{i}kL_{n-1}}, \quad (r_n,\theta_n)\in\mathfrak{a}_n,\\ u(r_n,\theta_n;n) &= u(r_n-L_n,\theta_n+\pi-\alpha_n;n+1)\mathrm{e}^{-\mathrm{i}kL_n}, \qquad (r_n,\theta_n)\in\mathfrak{b}_n, \end{aligned} \tag{3.4}$$

which suggest that the best place to switch from the coordinates (r_n,θ_n) to (r_{n-1},θ_{n-1}) is the ray $\mathfrak{a}_n$, and that the ray $\mathfrak{b}_n$ is the best place to switch from (r_n,θ_n) to (r_{n+1},θ_{n+1}).

Substitution of (3.1) into the Helmholtz equation shows that the amplitude $u(r_n,\theta_n;n)$ must obey the equations

$$\frac{r_n^2}{2}\frac{\partial^2 u}{\partial r_n^2} + r_n\left(\frac{1}{2}+\mathrm{i}kr_n\right)\frac{\partial u}{\partial r_n} + \frac{1}{2}\frac{\partial^2 u}{\partial\theta_n^2} + \frac{\mathrm{i}kr_n}{2}u = 0, \tag{3.5}$$

written in the coordinates (r_n,θ_n) with any admissible index. Also, the amplitude $u(r_\mu,\theta_\mu;\mu)$ must obey the radiation and interface conditions

$$u(r_\mu,\theta_\mu;\mu) = o(1), \text{as} \quad r_\mu\to\infty \quad \theta_\mu\neq\phi, \tag{3.6}$$

and

$$\begin{aligned} &u(r_\mu,\phi+0;\mu) - u(r_\mu,\phi-0;\mu) = 1,\\ &\frac{\partial u(r_\mu,\phi+0;\mu)}{\partial\theta_\mu} = \frac{\partial u(r_\mu,\phi-0;\mu)}{\partial\theta_\mu}, \end{aligned} \tag{3.7}$$

formulated in the coordinates (r_μ,θ_μ) associated with the suppressed index μ from (3.1). Finally, the amplitude $u(r_n,\theta_n;n)$ must obey the boundary conditions

$$\begin{aligned} &\frac{\partial u}{\partial\theta_n} + \mathrm{i}kr_nB_{n-1}u = 0 \quad \text{if } (r_n,\theta_n)\in\mathfrak{g}_{n-1},\\ &-\frac{\partial u}{\partial\theta_n} + \mathrm{i}kr_nB_nu = 0 \quad \text{if } (r_n,\theta_n)\in\mathfrak{g}_n, \end{aligned} \tag{3.8}$$

where n takes any integer value assuming that the coefficients B_n are extended beyond the interval $1 \leqslant n \leqslant N$ by the periodicity convention $B_{n+N} = B_n$ similar to (2.1).

3.2. Computation of $u_{\mu,\phi}(r,\theta;\mu)$ in the wedge $\mathfrak{D}_\mu$ with partially known boundary values

We start from the assumption that the amplitude $u(r_\mu,\theta_\mu;\mu)$ is already known on the part of the boundary of $\mathfrak{D}_\mu$ which does not coincide with the polygon Γ. To be precise, we observe that the boundary of $\mathfrak{D}_\mu$ consists of two sides $\mathfrak{g}_{\mu-1}$ and $\mathfrak{g}_\mu$ of the polygon Γ and of two rays $\mathfrak{a}_\mu$ and $\mathfrak{b}_\mu$, shown in Fig. 1 by dashed lines. On the sides of the polygon the amplitude $u(r_\mu,\theta_\mu;\mu)$ must obey the impedance boundary conditions (3.8), but on the rays $\mathfrak{a}_\mu$ and $\mathfrak{b}_\mu$ this amplitude may not be known until the *Problem-I* is solved. However, we assume that this amplitude is pre-defined on the rays $\mathfrak{a}_\mu$ and $\mathfrak{b}_\mu$, and using this information we calculate $u(r_\mu,\theta_\mu;\mu)$ inside the wedge $\mathfrak{D}_\mu$.

In [5] we introduced a version of the random walk method which provides an explicit description of the diffracted fields in a half plane with a piece-wise constant boundary impedance. Although the half plane can be considered as a very special wedge $0 < \theta < \pi$, it is easy to see that the method from [5] can be applied to the above mentioned problem in the wedge $\mathfrak{D}_\mu$ of arbitrary angle. As a result we obtain the representation of $u(r_\mu,\theta_\mu;\mu)$ in the probabilistic form

$$u(r_\mu,\theta_\mu;\mu) = \mathbf{E}\left\{ u(\xi_{t_1},\eta_{t_1};\mu)\mathrm{e}^{\mathrm{i}kS(t_1)} + \sum_{v=1}^{\tau_v<t_1} \delta_v(\phi)\mathrm{e}^{\mathrm{i}kS(\tau_v)} \right\}, \tag{3.9}$$

the exact meaning of which is explained below.

The mathematical expectation $\mathbf{E}$ is computed over the trajectories of stochastic processes ξ_t, η_t and $S(t)$ which are launched at the time $t = 0$ from the initial positions

$$\xi_0 = r_\mu, \qquad \eta_0 = \theta_\mu, \qquad S(0) = 0, \tag{3.10}$$

and evolve thereafter under the control of the stochastic differential equations

$$\mathrm{d}\xi_t = \xi_t \mathrm{d}w_t^1 + \xi_t\left(\frac{1}{2} + \mathrm{i}k\xi_t\right)\mathrm{d}t, \tag{3.11}$$

$$\mathrm{d}\eta_t = \begin{cases} \mathrm{d}t & \text{if } (\xi_t,\eta_t) \in \mathfrak{g}_{\mu-1}, \\ -\mathrm{d}t & \text{if } (\xi_t,\eta_t) \in \mathfrak{g}_\mu, \\ \mathrm{d}w_t^2 & \text{otherwise}, \end{cases} \tag{3.12}$$

and

$$\mathrm{d}S(t) = \frac{1}{2}\xi_t \mathrm{d}t + \begin{cases} \xi_t B_{\mu-1}\,\mathrm{d}t & \text{if } (\xi_t,\eta_t) \in \mathfrak{g}_{\mu-1}, \\ \xi_t B_\mu\,\mathrm{d}t & \text{if } (\xi_t,\eta_t) \in \mathfrak{g}_\mu, \\ 0 & \text{otherwise}, \end{cases} \tag{3.13}$$

where w_t^1 and w_t^2 are standard Brownian motions independent of each other.

The angular motion running inside the interval $[0,\alpha_\mu]$ touches the fixed point $\eta = \phi$ at the times $t = \tau_v$ enumerated by the index $v \geqslant 1$ which determines the factors $\delta_v(\phi)$ by the rules

$$\delta_v(\phi) = \begin{cases} 1 & \text{if } \phi < \eta_{\tau_v-0}, \quad \eta_{\tau_v+0} < \phi, \\ -1 & \text{if } \phi > \eta_{\tau_v-0}, \quad \eta_{\tau_v+0} > \phi, \\ 0 & \text{otherwise}. \end{cases} \tag{3.14}$$

Finally, all of the processes stop at the exit time $t = t_1$ defined as the first time when the point (ξ_t,η_t) touches either of the manifolds $\mathfrak{a}_\mu$ or $\mathfrak{b}_\mu$ defined by the analytic equations (2.8).

It is clear that the angular motion η_t is contained in the segment $0 \leqslant \eta_t \leqslant \alpha_\mu$ of the real axis, and that the radial motion ξ_t leaves the real axis immediately after launch and then runs inside the first quarter of the

complex plane drifting towards the unreachable point $\xi = \mathrm{i}/2k$. The fact that ξ_t runs in the complex plane implies that $\mathfrak{g}_{n-1}$ and $\mathfrak{g}_n$ in (3.12) should be considered as complex manifolds described by the analytic equations (2.7).

As mentioned above the radial motion ξ_t is contained in the first quarter of the plane $0 < \xi_t < \pi/2$ and drifts towards the point $\xi = \mathrm{i}/2k$. This guarantees that the exponents in (3.9) decay as the running time of the motions increases, which provides the convergence of (3.9). It is also clear that if the initial position (ξ_0,η_0) is located infinitesimally close to the boundary of the wedge $\mathfrak{D}_\mu$, then there is 100% probability that this boundary is hit by the trajectory of (ξ_t,η_t) in infinitesimally short time. This property guarantees that the mathematical expectation (3.9) satisfies the boundary conditions on the rays $\mathfrak{a}_\mu$ and $\mathfrak{b}_\mu$, as well as on the sides $\mathfrak{g}_{\mu-1}$, $\mathfrak{g}_\mu$ of the polygon Γ.

3.3. Computation of $u_\mu(r,\theta)$ in the wedge $\mathfrak{D}_\mu$

Expression (3.9) cannot be accepted as a solution of the problem because its right-hand side involves yet unknown values $u(\xi_{t_1},\eta_{t_1};\mu)$. These values can certainly be represented by the probabilistic formulas like (3.9), but using the coordinates (r_μ,θ_μ) we will not be able to enforce the boundary conditions on any of the segments $\mathfrak{g}_m$ except for $\mathfrak{g}_{\mu-1}$ and $\mathfrak{g}_\mu$, which are only parts of the boundary of $\mathfrak{D}_\mu$. Indeed, on any such segments the coordinates (r_μ,θ_μ) must be related by $r_\mu\cos(\theta_\mu - \zeta) = h$, where h and ζ are real constants. But the random motions ξ_t and η_t controlled by (3.11) and (3.12) can never satisfy equation $\xi_t\cos(\eta_t - \zeta) = h$ with real h and ζ, because η_t is always real while ξ_t is always complex.

From the above we see that the values of $u(\xi_{t_1},\eta_{t_2};\mu)$ in the right-hand side of (3.9) can not be represented by a probabilistic expression like (3.9) in the coordinates (r_μ,θ_μ). However, in another coordinate set these values can also be computed by probabilistic formulas similar to (3.9)–(3.14).

From the definition of the exit time t_1 it follows that the exit point (ξ_τ,η_τ) is located on either of the manifolds $\mathfrak{a}_\mu$ or $\mathfrak{b}_\mu$, which were mentioned in Section 3.1 as convenient places for switching from the coordinates (r_μ,θ_μ) to the coordinates $(r_{\mu-1},\theta_{\mu-1})$ or $(r_{\mu+1},\theta_{\mu+1})$, respectively. Then, applying conversion formulas (3.4) we obtain the identities

$$u(\xi_{t_1},\eta_{t_1};\mu) = \begin{cases} u(\xi_{t_1} - L_{\mu-1},\ \eta_{t_1} + \alpha_{\mu-1} - \pi;\ \mu-1)\ \mathrm{e}^{-\mathrm{i}kL_{\mu-1}} & \text{if } (\xi_{t_1},\eta_{t_1}) \in \mathfrak{a}_\mu, \\ u(\xi_{t_1} - L_\mu,\ \eta_{t_1} + \pi - \alpha_\mu;\ \mu+1)\ \mathrm{e}^{-\mathrm{i}kL_\mu} & \text{if } (\xi_{t_1},\eta_{t_1}) \in \mathfrak{b}_\mu, \end{cases} \tag{3.15}$$

with the right-hand sides which can be computed by the formulas ((3.9)–(3.14)) adapted to the wedges $\mathfrak{D}_{\mu-1}$ and $\mathfrak{D}_{\mu+1}$. For example, the value of $u(\xi_{t_1} - L_{\mu-1},\eta_{t_1} + \alpha_{\mu-1} - \pi;\mu-1)$ from first line of the right-hand part of (3.15) can be represented as the mathematical expectation

$$u(\xi_{t_1} - L_{\mu-1},\ \eta_{t_1} + \alpha_{\mu-1} - \pi;\ \mu-1) = \mathbf{E}\{u(\xi_{t_2},\eta_{t_2};\mu-1)\mathrm{e}^{\mathrm{i}kS(t_2)}\}, \tag{3.16}$$

computed over the trajectories of the stochastic processes ξ_t, η_t and $S(t)$ which are launched at the time $t = t_1$ from the initial positions

$$\xi_{t_1} = \xi_{t_1} - L_{\mu-1}, \qquad \eta_0 = \eta_{t_1} + \alpha_{\mu-1} - \pi, \qquad S(0) = S(t_1), \tag{3.17}$$

controlled thereafter by the stochastic equations (3.11)–(3.13) with μ replaced by $(\mu-1)$, and stopped at the exit time $t = t_2$ when the trajectory of (ξ_t,η_t) hits either of the rays $\mathfrak{a}_{\mu-1}$ or $\mathfrak{b}_{\mu-1}$.

It should be explained why the right-hand side of (3.16) does not contain the second term similar to that in (3.9). This difference is related to the interface conditions (3.7) which are formulated on the ray $\theta_\mu = \phi$ originating from the vertex of the wedge $\mathfrak{D}_\mu$. The random motion (ξ_t,η_t) involved in (3.9) intersects that ray at the times $t = \tau_v$, and each crossing contributes to the right-hand side of (3.9). However, the random motion involved in (3.16) never intersects that ray because of the following: (a) functions ξ_t and η_t are considered in (3.16) as coordinates of a moving point in the $(\mu-1)$-th coordinate system $(r_{\mu-1},\theta_{\mu-1})$, where the ray $\theta_\mu = \phi$ is described by the equation $r_{\mu-1}\sin(\theta_{\mu-1} - \zeta) = h$, where h and ζ are real constants; (b) the angular motion η_t is confined to the real axis, while the radial motion ξ_t is always complex-valued; (c) such ξ_t and η_t can not satisfy equation $\xi_t\sin(\eta_t - \zeta) = h$ with real h and ζ.

To complete the second step we evaluate the second line of (3.15) by the formula

$$u(\xi_{t_1} - L_\mu,\ \eta_{t_1} + \pi - \alpha_\mu;\ \mu + 1) = \mathbf{E}\{u(\xi_{t_2}, \eta_{t_2}; \mu + 1)\mathrm{e}^{\mathrm{i}kS(t_2)}\}, \tag{3.18}$$

where ξ_t, η_t and $S(t)$ are launched at the time $t = t_1$ from the initial positions

$$\xi_{t_1} = \xi_{t_1} - L_\mu, \qquad \eta_0 = \eta_{t_1} + \pi - \alpha_\mu, \qquad S(0) = S(t_1), \tag{3.19}$$

run thereafter under the control of Eqs. (3.11)–(3.13) with μ replaced by $(\mu + 1)$, and stop at the exit time $t = t_2$ when it hits either of the rays $\mathfrak{a}_{\mu+1}$ or $\mathfrak{b}_{\mu+1}$. Then, the (3.16)–(3.19) with (3.9) we arrive at the expression

$$u(r_\mu, \theta_\mu; \mu) = \mathbf{E}\left\{\sum_{v=1}^{\tau_v < t_1} \delta_v(\phi)\mathrm{e}^{\mathrm{i}kS(\tau_v)} + u(\xi_{t_2}, \eta_{t_2}; \mu_1)\mathrm{e}^{\mathrm{i}k[S(t_2) - \Lambda_1]}\right\}, \tag{3.20}$$

where $\mu_1 = \mu \pm 1$ and $\Lambda_1 = \Lambda_{\mu_1}$. The exit point (ξ_{t_2}, η_{t_2}) belongs to one of the half-lines $\mathfrak{a}_{\mu_1}$ or to $\mathfrak{b}_{\mu_1}$, which are convenient places for switching from the coordinates $(r_{\mu_1}, \theta_{\mu_1})$ either back to the coordinates (r_μ,θ_μ) or to the coordinates $(r_{\mu\pm2},\theta_{\mu\pm2})$, respectively.

It is obvious that the value of $u(\xi_{t_2}, \eta_{t_2}; \mu_1)$ which appears in the right-hand side of (3.20) can be evaluated by formulas similar to (3.20), and repeating the recursion infinitely many times, we eventually arrive at the expression

$$u(r, \theta; \mu) = \mathbf{E}\left\{\sum_{v=1}^{\infty} \delta_v(\phi; \mu) \exp[\mathrm{i}kS(\tau_v) - \mathrm{i}k\Lambda(\tau_v)]\right\}, \tag{3.21}$$

where the mathematical expectation is computed over trajectories of the stochastic processes n_t, ξ_t, η_t, $\Lambda(t)$ and $S(t)$ which launch at the time $t = 0$ from the initial positions

$$n_0 = \mu, \quad \xi_0 = r_\mu, \quad \eta_0 = \theta_\mu, \quad \Lambda(0) = S(0) = 0, \tag{3.22}$$

and run thereafter under the rules described below.

The process n_t takes integer values which change only at the time when the point (ξ_t,η_t) reaches one of the rays $\mathfrak{a}_n$ or $\mathfrak{b}_n$. More precisely, the evolution of n_t is described by the rules

$$n_{t+0} - n_t = \begin{cases} +1 & \text{if } (\xi_t, \eta_t) \in \mathfrak{a}_{n_t}, \\ -1 & \text{if } (\xi_t, \eta_t) \in \mathfrak{b}_{n_t}, \\ 0 & \text{otherwise}, \end{cases} \tag{3.23}$$

which suggests that n_t should be interpreted as an index of the currently used coordinate system.

The angular motion η_t is controlled by the stochastic equations

$$\mathrm{d}\eta_t = \begin{cases} -\mathrm{d}t & \text{if } (\xi_t, \eta_t) \in \mathfrak{g}_{n_t}, \\ \mathrm{d}t & \text{if } (\xi_t, \eta_t) \in \mathfrak{g}_{n_t - 1}, \\ \alpha_{n-1} - \pi & \text{if } (\xi_t, \eta_t) \in \mathfrak{a}_{n_t}, \\ \pi - \alpha_n & \text{if } (\xi_t, \eta_t) \in \mathfrak{b}_{n_t}, \\ \mathrm{d}w_t^2 & \text{otherwise}, \end{cases} \tag{3.24}$$

where w_t^2 is the standard Brownian motion. These equations coincide with (3.12) as long as the point (ξ_t,η_t) is located inside the wedge $\mathfrak{D}_{n_t}$, but Eq. (3.24) have two additional lines which describe the behavior of η_t at the time of the switch from the n_tth to the neighboring $(n_t \pm 1)$-th coordinates.

The angular motion η_t together with the index n_t determine the factor $\delta_v(\phi;\mu)$ by the rules

$$\delta_v(\phi; \mu) = \begin{cases} 1 & \text{if } \phi < \eta_{\tau_v - 0}, \quad \eta_{\tau_v + 0} < \phi,\ n_t = \mu, \\ -1 & \text{if } \phi > \eta_{\tau_v - 0}, \quad \eta_{\tau_v + 0} > \phi,\ n_t = \mu, \\ 0 & \text{otherwise}, \end{cases} \tag{3.25}$$

where v enumerates the times $t = \tau_v$ when $n_t = \mu$ and the motion η_t touches the point $\eta = \phi$.

The radial motion ξ_t and the stochastic processes $\Lambda(t)$ are closely related to each other and are controlled by the stochastic equations

$$\Lambda_{t+\mathrm{d}t} - \Lambda_t = \begin{cases} L_{n_t-1} & \text{if } (\xi_t, \eta_t) \in \mathfrak{a}_{n_t}, \\ L_{n_t} & \text{if } (\xi_t, \eta_t) \in \mathfrak{b}_{n_t}, \\ 0 & \text{otherwise.} \end{cases} \tag{3.26}$$

and

$$\xi_{t+\mathrm{d}t} - \xi_t = \xi_t \mathrm{d}w_t^1 + \xi_t\left(\tfrac{1}{2} + \mathrm{i}k\xi_t\right)\mathrm{d}t - (\Lambda_{t+\mathrm{d}t} - \Lambda_t), \tag{3.27}$$

where w_t^1 is the standard Brownian motion. It is obvious that ξ_t has jumps at the times when the index n_t changes, and from the observation that these jumps are always real, it follows that ξ_t is contained in the upper half-plane $\mathrm{Im}(\xi_t) > 0$ and has a drift towards the point $\xi = \mathrm{i}/2k$.

Finally, $S(t)$ is a stochastic process defined by the equation

$$S_{t+\mathrm{d}t} - S_t = \frac{1}{2}\xi_t \mathrm{d}t + \begin{cases} \xi_t B_{n_t-1}\mathrm{d}t & \text{if } (\xi_t, \eta_t) \in \mathfrak{g}_{n_{t-1}}, \\ \xi_t B_{n_t}\mathrm{d}t & \text{if } (\xi_t, \eta_t) \in \mathfrak{g}_{n_t}, \\ 0 & \text{otherwise,} \end{cases} \tag{3.28}$$

which is practically identical to (3.13).

3.4. Computation of the field $U_{\mu,\phi}(r,\theta)$ anywhere

Formulas 3.1 and (3.21)–(3.28) represent the solution of *Problem-I* inside the wedge $\mathfrak{D}_\mu$ singled out by the interface conditions (2.24) and, due to the analyticity inherited from the properties of the Helmholtz equation, it has to admit analytic continuation outside $\mathfrak{D}_\mu$. However, the above mentioned formulas can not be straightforwardly used outside $\mathfrak{D}_\mu$, because they do not provide smoothness of the field $U_{\mu,\phi}(r,\theta)$ on the rays $\mathfrak{a}_\mu$ and $\mathfrak{b}_\mu$. Indeed, suppose that $P_\pm = (r_\mu, \alpha_\mu \pm 0)$ are two points given in the μth coordinate system. We assume that $r_\mu > L_\mu$ so that these points are located infinitesimally close to the ray $\mathfrak{b}_\mu$, but P_+ is placed inside $\mathfrak{D}_\mu$, while P_- is placed outside $\mathfrak{D}_\mu$. To see that the mathematical expectations (3.16) corresponding to the points $P_\pm$ may not coincide it suffices to observe that a small difference in the locations of these points causes a significant difference in the synchronization of the stochastic processes controlled by the Eqs. (3.23)–(3.28) and the initial conditions (3.22). Thus, (3.24) imply that the angular motions $\eta_t^\pm$ corresponding to $P_\pm$ have equal chances to start motion in the direction towards $\mathfrak{D}_\mu$. However, if η_t^- goes there, then the corresponding index n_t^- controlled by (3.23) remains unchanged because $\mathfrak{b}_\mu$ is not crossed, but if η_t^+ goes there, then n_t^+ increases, and the difference between n_t^+ and n_t^- drastically affects the future of all stochastic processes involved in (3.21).

To get a correct continuation of the field $U_{\mu,\phi}(r,\theta)$ out of the wedge $\mathfrak{D}_\mu$ it is instructive to observe that this continuation has already been implicitly employed in Section 3.3 as a critical technical tool for the computation of the amplitude $u_{\mu,\phi}(r,\theta)$ at the points (r,θ) located inside $\mathfrak{D}_\mu$. Thus, we first represented $u(r_\mu,\theta_\mu;\mu)$ through its own values on the rays $\mathfrak{a}_\mu$ and $\mathfrak{b}_\mu$, which belong to the boundary of $\mathfrak{D}_\mu$ but, at the same time, are located inside of the adjacent wedges $\mathfrak{D}_{mu-1}$ and $\mathfrak{D}_\mu$. Then, to compute $u(r_\mu,\theta_\mu;\mu)$ on $\mathfrak{a}_\mu$, we switched from the coordinates (r_μ,θ_μ) to the coordinates $(r_{\mu-1},\theta_{\mu-1})$ associated with the wedge $\mathfrak{D}_{\mu-1}$. Similarly, on the ray $\mathfrak{b}_\mu$ we switched from the coordinates (r_μ,θ_μ) to the coordinates $(r_{\mu+1},\theta_{\mu+1})$ used in $\mathfrak{D}_{\mu+1}$. Using the new coordinates, we were able to represent the value of $U_{\mu,\phi}(r,\theta)$ through the values of the same field on $\mathfrak{a}_{\mu-2}$ and $\mathfrak{b}_{\mu+1}$, and continuing the recursion we arrived at the representation (3.21)–(3.28).

The last observation implies that the continuation of the field $U_{\mu,\phi}(r,\theta)$ outside the wedge $\mathfrak{D}_\mu$ can be carried out by the multi-step algorithm from Section 3.3. In the first stage, this field is continued from $\mathfrak{D}_\mu$ to the adjacent parts

$$\begin{aligned}\mathfrak{D}_{\mu-1}\setminus\mathfrak{D}_{\mu}&=\{r_{\mu-1},\theta_{\mu-1}:\ 0<\theta_{\mu-1}<\alpha_{\mu-1}-\pi\},\\ \mathfrak{D}_{\mu+1}\setminus\mathfrak{D}_{\mu}&=\{r_{\mu+1},\theta_{\mu+1}:\ \pi<\theta_{\mu+1}<\alpha_{\mu+1}\},\end{aligned}\tag{3.29}$$

of the wedges $\mathfrak{D}_{\mu+1}$ and $\mathfrak{D}_{\mu-1}$. In these domains $U_{\mu,\phi}(r,\theta)$ is represented as the mathematical expectations

$$\begin{aligned}U_{\mu,\phi}&=\mathrm{e}^{\mathrm{i}kr_{\mu-1}}\mathbf{E}\left\{\sum_{v=1}^{\infty}\delta_v(\phi;\mu)\exp(\mathrm{i}k[S(\tau_v)-\Lambda(\tau_v)])\right\},\quad 0<\theta_{\mu-1}<\alpha_{\mu-1}-\pi,\\ U_{\mu,\phi}&=\mathrm{e}^{\mathrm{i}kr_{\mu+1}}\mathbf{E}\left\{\sum_{v=1}^{\infty}\delta_v(\phi;\mu)\exp(\mathrm{i}k[S(\tau_v)-\Lambda(\tau_v)])\right\},\quad \pi<\theta_{\mu+1}<\alpha_{\mu+1},\end{aligned}\tag{3.30}$$

where all the notation retains its meaning from (3.21), except that here the initial positions of the random processes are defined by the formulas

$$\begin{aligned}n_0&=\mu-1,\quad \xi_0=r_{\mu-1},\quad \eta_0=\theta_{\mu-1},\quad \Lambda(0)=S(0)=0,\\ n_0&=\mu+1,\quad \xi_0=r_{\mu+1},\quad \eta_0=\theta_{\mu+1},\quad \Lambda(0)=S(0)=0,\end{aligned}\tag{3.31}$$

which correspond to the upper and the lower lines of (3.30), respectively.

Formulas (3.30) and (3.1), (3.21) together cover three overlapping domains $\mathfrak{D}_{\mu-1}$–$\mathfrak{D}_{\mu+1}$, and in the next stage they can be extended to the next adjacent sectors $\mathfrak{D}_{\mu-2}\setminus\mathfrak{D}_{\mu-1}$ and $\mathfrak{D}_{\mu+2}\setminus\mathfrak{D}_{\mu+1}$. Continuing the outlined process we eventually arrive at a representation of the field $U_{\mu,\phi}(r,\theta)$ which is valid in the infinite angular domain $-\infty<\theta<\infty$ and has the structure

$$U_{\mu,\phi}(r,\theta)=\mathrm{e}^{\mathrm{i}kr_{\bar{\mu}}}\mathbf{E}\left\{\sum_{v=1}^{\infty}\delta_v(\phi;\mu)\exp(\mathrm{i}k[S(\tau_v)-\Lambda(\tau_v)])\right\},\tag{3.32}$$

where all the notation retains its meaning from (3.21), except that the stochastic processes start from the positions

$$n_0=\bar{\mu},\quad \xi_t=r_{\bar{\mu}},\quad \eta_0=\theta_{\bar{\mu}},\quad S(0)=\Lambda(0)=0,\tag{3.33}$$

determined through the index

$$\bar{\mu}=\begin{cases}\min\{m:\ P\in\mathfrak{D}_m\} & \text{if } \theta_\mu>\alpha_\mu,\\ \min\{m:\ P\in\mathfrak{D}_m\} & \text{if } \theta_\mu<0,\\ \mu, & \text{if } \quad 0\leqslant\theta_\mu\leqslant\alpha_\mu\end{cases}\tag{3.34}$$

which can be interpreted as the index of the wedge $\mathfrak{D}_{\bar{\mu}}$ containing $P=(r,\theta)$, closest to $\mathfrak{D}_\mu$.

4. Examples

To verify the feasibility of the obtained probabilistic solution of the problem of diffraction by a convex polygon, we conducted numerical simulations of the wave fields generated by an incident plane wave $U_*=\mathrm{e}^{-\mathrm{i}r\cos(\theta-\theta_*)}$ from a short 'bullet'-like pentagon shown in Fig. 3 and by a longer 'missile'-like pentagon shown in Fig. 6. In both cases, the impedances of the faces were chosen as $B_1=0$, $B_2=2$, $B_3=1$, $B_4=0$, and $B_5=3$. The vertices are located by standard Cartesian coordinates with the origin at O_1.

Figs. 4 and 5 show the magnitudes and the phases of the total and the geometric fields generated due to the scattering by the short pentagon in Fig. 3. The wave fields were computed along three circles with their centers at the point $C=(-3,0)$ in the middle of the polygon. The top diagrams show wave fields along the circle of

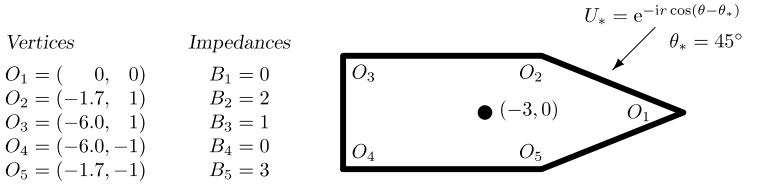

Fig. 3. Scattering by a 'short bullet'.

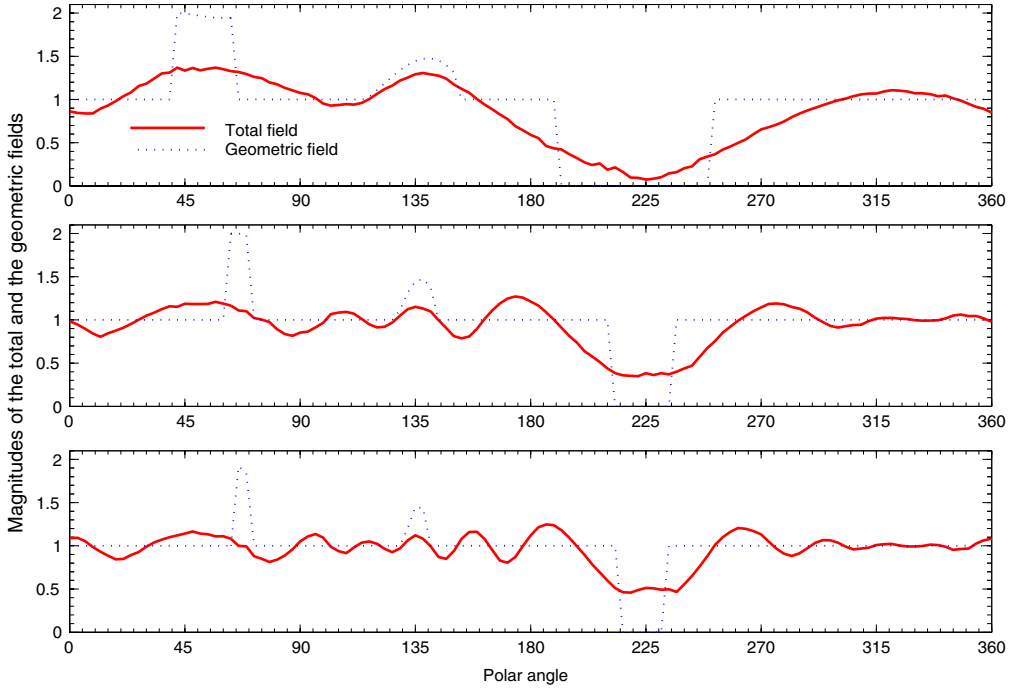

Fig. 4. Magnitudes of the total and geometric fields around a 'short bullet'.

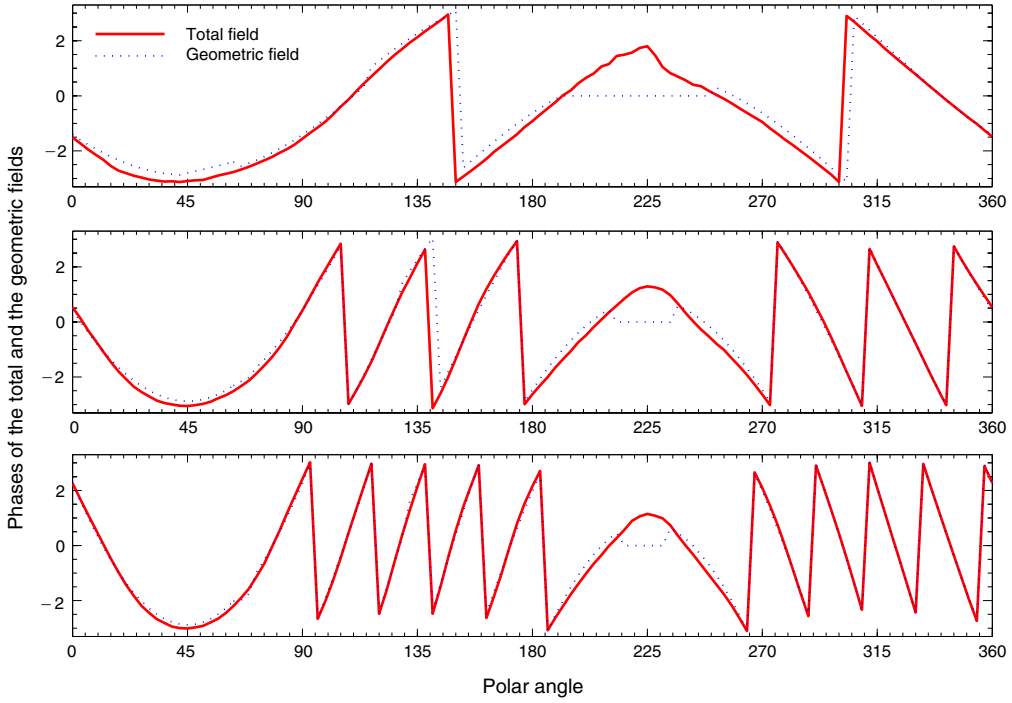

Fig. 5. Phases of the total and geometric fields around a 'short bullet'.

radius $R_1 = 5$, the middle diagrams show wave fields along the circle with $R_2 = R_1 + 2\pi$, and the bottom diagrams show the field along the circle with radius $R_3 = R_2 + 2\pi$. In all of the diagrams the dashed lines correspond to the geometric fields which comprise the incident and reflected plane waves, and the solid lines correspond to the total wave fields, which include the diffracted fields.

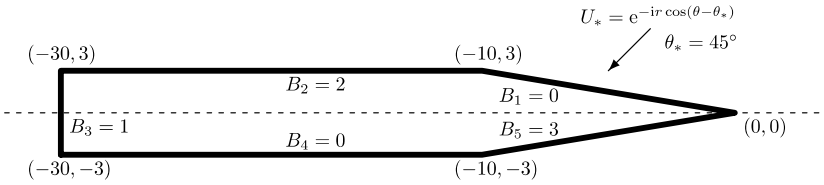

Fig. 6. Scattering by a 'long missile'.

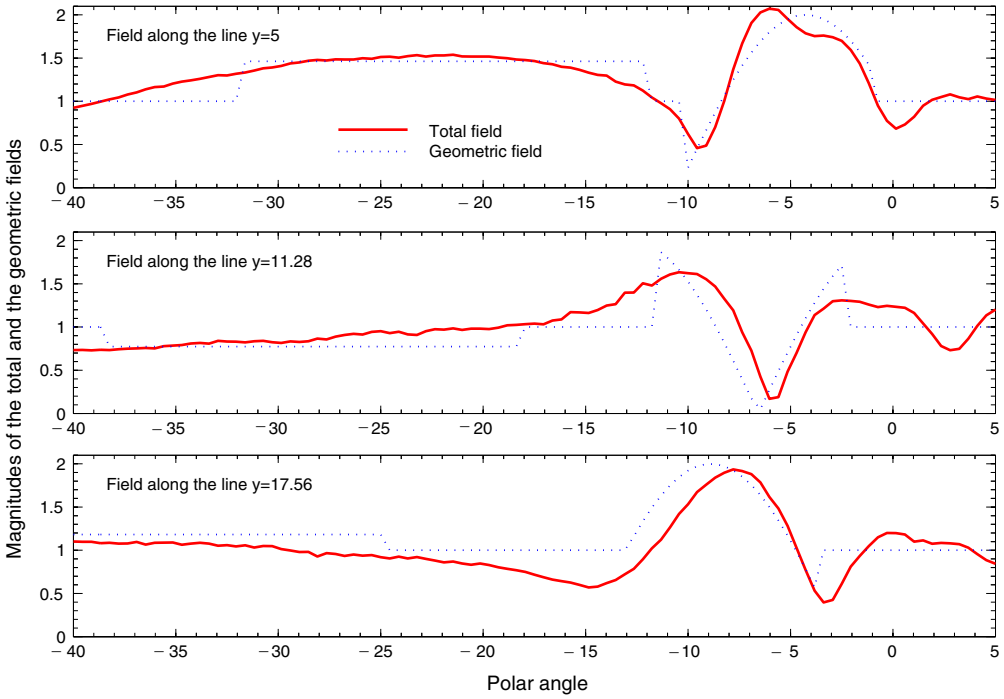

Fig. 7. Magnitudes of the total and geometric fields above the 'missile'.

All the numerical results were obtained by the approximation of the mathematical expectation (3.32) by the average of 1000 sample values of the functional computed along discrete random motions with the time step $\Delta = 0.01$. The standard deviation of the samples did not exceed the level $D = 0.5$, which suggests good convergence and stability of the solution.

The diagrams in Figs. 4 and 5 clearly demonstrate the expected behavior of the simulated wave fields generated by the interaction of an incident plane wave with the polygon. Thus, in the absence of the scatterer, the total wave field along the circles would have a unit magnitude and the sinusoidal phase. In the presence of the object in Fig. 3 the laws of geometric optics predict a shadow zone around the ray $\theta = 225°$, and two zones illuminated by the waves reflected from the sides O_1O_2 and O_2O_3. It is also expected that the fine structure of the scatterer should be less observable with increasing distance from it. These physically justified predictions are soundly confirmed by the presented graphs. Thus, at a short distance from the object (the top diagrams) the shadow is deep and the magnitude of the total field almost vanishes near the ray $\theta = 225°$, which explains some irregularity of the behavior of the corresponding phase. However, in the middle and the bottom diagrams the shadow is not deep and the total wave field there is far from vanishing.

The bottom diagrams also make it obvious that the disturbance caused by the reflection from the side O_2O_3 spreads over several peaks which makes it difficult to recover the location of this side based only on the observation of the total wave field, at the distance of only 2.5 wave lengths.

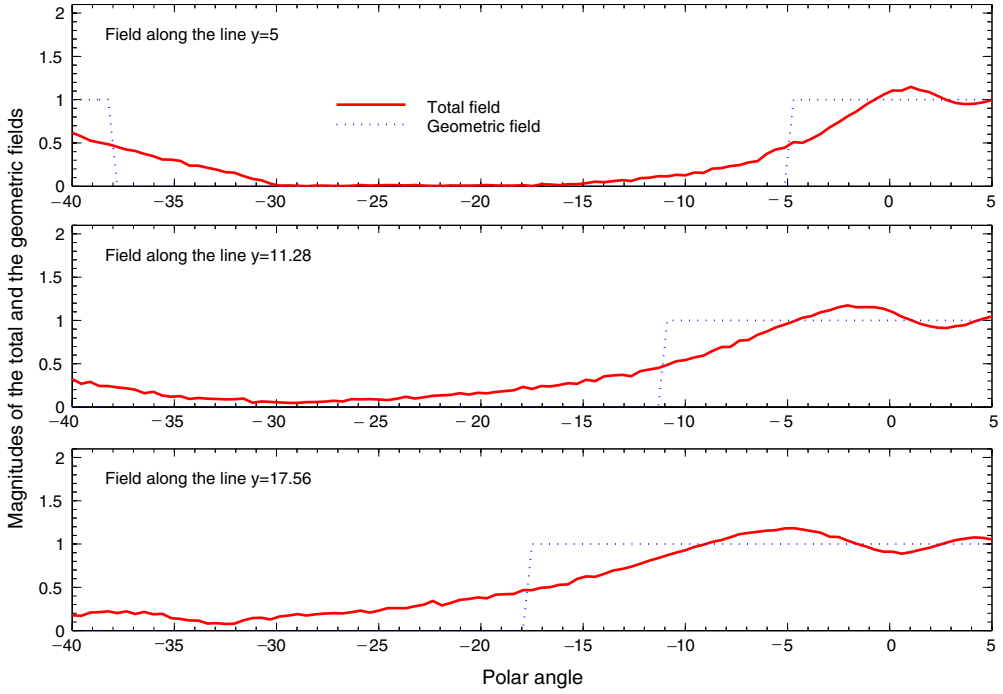

Fig. 8. Phases of the total and geometric fields under the 'missile'.

It is also interesting to compare the influence of the waves reflected by the sides O_1O_2 and O_2O_3, the first of which has the length $L_1 = 2$, which is less than 30% of the wavelength, while the second side has the length $L_2 = 4.3$ which is about 70% of the wavelength. According to the principles of physical optics, the smaller side should have considerably less noticeable impact on the total field, and this is confirmed by all of the presented diagrams which show noticeable differences between the fluctuations caused by the sides O_2O_3 and O_1O_2.

The results of the numerical simulations of scattering by a longer 'missile'-like pentagon in Fig. 6 are shown in Figs. 7 and 8 which show the magnitudes of the total and the geometric fields along several horizontal lines located above and below the scatterer.

In Fig. 7 the top diagram corresponds to the wave fields on the line $y = 5$, which passes along the close distance $d = 2$ from the scatterer. The middle and the bottom diagrams of this figure show the fields on the lines $y = 5 + 2\pi$ and $y = 5 + 4\pi$, moved further away by one and two wavelengths, respectively. The similarly organized Fig. 8 shows the wave fields along the lines $y = -5$, $y = -5 - 2\pi$, and $y = -5 - 4\pi$ located below the scatterer. As in the previous case, the results presented in Figs. 7 and 8 agree well with the expectations based on common sense and the geometrical theory of diffraction.

5. Conclusion

The probabilistic approach to wave propagation and diffraction surveyed in [4] made it possible to obtain explicit solutions of a number of difficult problems of diffraction, including the scalar problem of diffraction by a plane angular sector [2] and the vector problem of diffraction of the electromagnetic wave by a wedge with anisotropic impedance faces [3]. Although these problems are notoriously difficult for analysis by conventional methods, the obtained probabilistic solutions appear to be simple, transparent, compatible with intuitive ideas about diffraction, and easy for numerical implementation. The advantages of the random walk approach become even more apparent when it is applied to problems with several diffraction points. Thus, in [5] we explicitly solved the problem of wave scattering in a half plane with a piece-wise constant impedance boundary condition, and the problem of diffraction by a finite line segment with different impedance sides. Here we take the next step and extend the random walk method to two-dimensional problems of diffraction by arbitrary

convex polygons with side-wise constant impedance boundary conditions. It is somewhat surprising that such a general problem may have an explicit solution, but the probabilistic method indeed delivers explicit expressions which are simple and transparent, and they compliment the ray approximation to produce the theoretically exact solution.

Acknowledgements

This research was supported by NSF Grant CMS-0408381 and by the DARPA/AFOSR FA 9550-0501-0111 contract.

References

[1] J.M.L. Bernard, Scattering by a three-part impedance plane: a new spectral approach, Q. J. Mech. Appl. Math. 58 (3) (2005).
[2] B.V. Budaev, D.B. Bogy, Diffraction by a plane sector, Proc. R. Soc. A. 460 (2052) (2004) 3529–3546.
[3] B.V. Budaev, D.B. Bogy, Diffraction of a plane electromagnetic wave by a wedge with anisotropic impedance faces, IEEE Trans. Antennas Propag. 54 (5) (2005) 1559–1567.
[4] B.V. Budaev, D.B. Bogy, Probabilistic approach to wave propagation, Radio Sci. 40 (6) (2005), paper #RS6S07.
[5] B.V. Budaev, D.B. Bogy, Two-dimensional problems of diffraction by finite collinear structures, J. Acoust. Soc. Am. 119 (2) (2005) 741–750.
[6] M. Freidlin, Functional integration and partial differential equations, The Annals of Mathematics Studies, Princeton University Press, Princeton, New Jersey, 1985.
[7] M. Idemen, A. Alkumru, On a class of functional equations of the Wiener-Hopf type and their applications in *n*-part scattering problems, IMA J. Appl. Math. 68 (2003) 563–586.
[8] K. Ito, H.P. McKean Jr., Diffusion Processes and Their Sample Paths, Springer-Verlag, Berlin, 1965.
[9] J.B. Keller, A geometric theory of diffraction, Calc. Var. Appl. (1958) 27–52.
[10] J.B. Keller, Diffraction by polygonal cylinders, Electromagn. Waves (1962) 129–137.
[11] J.H. Poincaré, Sur la polarisation par diffraction, Acta Math. 16 (1892) 297–339.
[12] J.H. Poincaré, Sur la polarisation par diffraction, Acta Math. 20 (1897) 313–355.
[13] A. Sommerfeld, Mathematische Theorie der Diffraction, Mathematische Annalen 47 (1896) 317–374.